LA-UR -76-1229

CONF-760825--14

TITLE: A NUMERICAL METHOD FOR TWO-DIMENSIONAL UNSTEADY REACTING FLOWS

AUTHOR(S): T. D. Butler, T-3
P. J. O'Rourke, T-3

SUBMITTED TO: "The Sixteenth (International) Symposium on Combustion" August 15-21, 1976 at Cambridge, Massachusetts.

MASTER

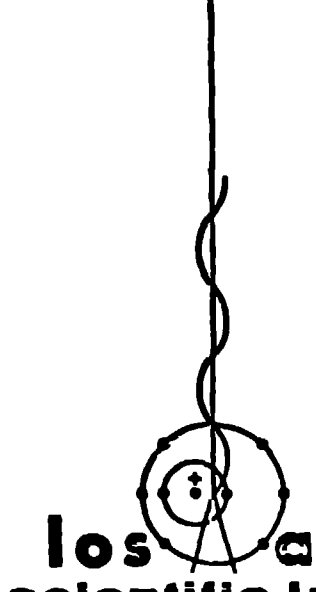

los alamos
scientific laboratory
of the University of California
LOS ALAMOS, NEW MEXICO 87544

An Affirmative Action/Equal Opportunity Employer

Form No. 836
St. No. 2629
1/75

UNITED STATES
ENERGY RESEARCH AND
DEVELOPMENT ADMINISTRATION
CONTRACT W-7405-ENG. 36

A NUMERICAL METHOD FOR TWO DIMENSIONAL UNSTEADY REACTING FLOWS

by

T. D. Butler and P. J. O'Rourke*
Theoretical Division
Los Alamos Scientific Laboratory
University of California
Los Alamos, New Mexico 87545

SUMMARY

In this paper we present a method that numerically solves the full two-dimensional, time-dependent Navier-Stokes equations with species transport, mixing, and chemical reaction between species. The generality of the formulation permits the solution of flows in which deflagrations, detonations, or transitions from deflagration to detonation are found. The solution procedure is embodied in the RICE computer program. RICE is an Eulerian finite difference computer code that uses the Implicit Continuous-fluid Eulerian (ICE) technique to solve the governing equations. We first present the differential equations of motion and the solution procedure of the RICE program.

Next, a method is described for artificially thickening the combustion zone to dimensions resolvable by the computational mesh. This is done in such a way that the physical flame speed and jump conditions across the flame front are preserved.

Finally, the results of two example calculations are presented. In the first, the artificial thickening technique is used to solve a one-dimensional laminar flame problem. In the second, the results of a full two-dimensional calculation of unsteady combustion in two connected chambers are detailed.

*This work was performed under the auspices of the Energy Research and Development Administration and the Naval Ordnance Station.

1. INTRODUCTION

The extreme complexity of the coupled fluid dynamic and chemical processes that occur in unsteady deflagrations has made difficult the detailed analysis of these flows in more than one space dimension. In this paper we present, and illustrate by means of example calculations, a method that numerically solves the full two-dimensional Navier-Stokes equations with species transport, mixing, and chemical reactions between species. The method has been successfully applied to the analysis of continuous wave HF/DF chemical lasers,[1] to the burning of propellant in liquid monopropellant guns,[2] and to combustion in internal combustion engines.[3] The generality of the formulation permits the solution of flows in which deflagrations, detonations, or transitions from deflagration to detonation are found.

The solution procedure is embodied in the RICE[4] computer program. RICE is an Eulerian finite difference computer code that uses a modified form of the Implicit Continuous-fluid Eulerian (ICE)[5] technique to eliminate the Courant sound speed criterion on the magnitude of the calculational time step. The implicit formulation is particularly effective in deflagration studies where material speeds may be far subsonic, and traditional

explicit methods would require prohibitively small time steps.

In Sections II and III, we present the differential equations of motion and the solution procedure of the RICE code. Section III briefly outlines a method by which numerical stability and increased accuracy are achieved in RICE. The procedure, which involves the explicit cancellation of certain low-order diffusional truncation errors, is fully described elsewhere.[6,7]

In many cases of practical interest, particularly in laminar flames, the flame thickness is small compared to the spatial resolution of the computing mesh. In Section IV, we introduce a technique for artificially thickening the combustion zone to dimensions resolvable by the mesh. This is done in such a way that the flame speed is still determined by physical diffusivities and reaction rates. This procedure is often not necessary for turbulent flames because of their significantly greater thickness compared to laminar ones.

Finally, the results of two series of calculations are presented. In the first series, the artificial thickening technique is used to compute a one-dimensional, steady-state laminar flame in which the reaction rate is governed by a single, second order Arrhenius law. In the second series, the results of a full two-dimensional calculation of unsteady combustion in two connected chambers are detailed.

II. The Governing Equations

The partial differential equations that govern the fluid dynamics, species mixing, and chemical reactions are presented in this section. They are written in cylindrical coordinates with axial symmetry and zero azimuthal velocity. The equations for plane coordinates are obtained by setting the radial distance r equal to unity and the normal stress component $\sigma_{\phi\phi}$ equal to zero. The terms with the parameter β account for turbulent transport effects as will be explained later; laminar flows require setting β equal to zero. Table I lists the definitions of the symbols used and indicates the quantities needed as input for the RICE solution procedure.

A. The Mixture Equations.

The mixture-mass conservation equation is

$$\frac{\partial \rho}{\partial t} + \frac{1}{r}\frac{\partial \rho v r}{\partial r} + \frac{\partial \rho u}{\partial z} = \frac{1}{r}\frac{\partial}{\partial r}\left(r\beta\frac{\partial \rho}{\partial r}\right) + \frac{\partial}{\partial z}\left(\beta\frac{\partial \rho}{\partial z}\right) \quad . \tag{1}$$

The momentum conservation equations are given by

$$\frac{\partial \rho v}{\partial t} + \frac{1}{r}\frac{\partial \rho v^2 r}{\partial r} + \frac{\partial \rho u v}{\partial z} = -\frac{\partial p}{\partial r} + \frac{1}{r}\frac{\partial \sigma_{rr} r}{\partial r} + \frac{\partial \sigma_{rz}}{\partial z} - \frac{\sigma_{\phi\phi}}{r} + \nu\left[\frac{1}{r}\left(r\beta\frac{\partial \rho}{\partial r}\right) + \frac{\partial}{\partial z}\left(\beta\frac{\partial \rho}{\partial z}\right)\right] + \rho\beta\left[\frac{\partial^2 v}{\partial r^2} + \frac{\partial^2 v}{\partial z^2}\right] \tag{2}$$

and

$$\frac{\partial \rho u}{\partial t} + \frac{1}{r}\frac{\partial \rho u v r}{\partial r} + \frac{\partial \rho u^2}{\partial z} = -\frac{\partial p}{\partial z} + \frac{1}{r}\frac{\partial \sigma_{rz} r}{\partial r} + \frac{\partial \sigma_{zz}}{\partial z} + u\left[\frac{1}{r}\frac{\partial}{\partial r}\left(r\beta\frac{\partial \rho}{\partial r}\right) + \frac{\partial}{\partial z}\left(\beta\frac{\partial \rho}{\partial z}\right)\right] + \rho\beta\left[\frac{\partial^2 u}{\partial r^2} + \frac{\partial^2 u}{\partial z^2}\right] \quad . \tag{3}$$

The internal energy equation is

$$\frac{\partial \rho I}{\partial t} + \frac{1}{r}\frac{\partial \rho v r I}{\partial r} + \frac{\partial \rho u I}{\partial z} = - p\left(\frac{1}{r}\frac{\partial v r}{\partial r} + \frac{\partial u}{\partial z}\right) + \sigma_{rr}\frac{\partial v}{\partial r} + \sigma_{rz}\left(\frac{\partial v}{\partial z} + \frac{\partial u}{\partial r}\right)$$

$$+ \sigma_{zz}\frac{\partial u}{\partial z} + \sigma_{\phi\phi}\frac{v}{r} + \frac{1}{r}\frac{\partial}{\partial r}(r q_r) + \frac{\partial}{\partial z}(q_z) + \dot{q}_c$$

$$+ I\left[\frac{1}{r}\frac{\partial}{\partial r}\left(r\beta\frac{\partial I}{\partial r}\right) + \frac{\partial}{\partial z}\left(\beta\frac{\partial \rho}{\partial z}\right)\right]$$

$$+ \rho\beta\left[\frac{\partial^2 I}{\partial r^2} + \frac{\partial^2 I}{\partial z^2}\right] . \qquad (4)$$

In these equations, the components of the viscous stress tensor for a Newtonian fluid are defined in the following manner:

$$\sigma_{rr} = 2\mu\frac{\partial v}{\partial r} + \lambda\left(\frac{1}{r}\frac{\partial v r}{\partial r} + \frac{\partial u}{\partial z}\right)$$

$$\sigma_{rz} = \mu\left(\frac{\partial u}{\partial r} + \frac{\partial v}{\partial z}\right)$$

$$\sigma_{zz} = 2\mu\frac{\partial u}{\partial z} + \lambda\left(\frac{1}{r}\frac{\partial v r}{\partial r} + \frac{\partial u}{\partial z}\right)$$

$$\sigma_{\phi\phi} = 2\mu\frac{v}{r} + \lambda\left(\frac{1}{r}\frac{\partial v r}{\partial r} + \frac{\partial u}{\partial z}\right) , \qquad (5)$$

where μ and λ are the first and second coefficients of viscosity, respectively.

Turbulence is modeled by the terms containing β. Here, we briefly outline the procedure that leads to the form of these terms; a more

complete description is given in Ref. (1). First, we consider each mean flow quantity, ζ, to be the sum of an ensemble averaged part $\overline{\zeta}$ and a fluctuating part ζ' (i.e., $\zeta = \overline{\zeta} + \zeta'$). Inserting these expressions into the laminar equations, we recover the usual mean flow terms plus the contributions from the fluctuating components. We approximate these latter terms by first neglecting fluctuations in the pressure p', the molecular diffusivities (e.g., μ'), and the chemical reaction rates. Then we assume that the flux approximation is valid. This is,

$$\overline{\zeta' u_i'} = - \beta \frac{\partial \overline{\zeta}}{\partial x_i}$$

where u_i is the velocity in the i^{th} coordinate direction and β is the turbulent diffusivity. This leads to the terms in Eqs. (1)-(4) that represent the diffusion of mass, momentum, and energy.

The energy flux components in Eq. (4) are given by

$$q_r = \kappa \frac{\partial T}{\partial r} + \sum_k \rho h_k D_k \frac{\partial}{\partial r}\left(\frac{\rho_k}{\rho}\right)$$

and

$$q_z = \kappa \frac{\partial T}{\partial z} + \sum_k \rho h_k D_k \frac{\partial}{\partial z}\left(\frac{\rho_k}{\rho}\right) \qquad (6)$$

where $h_k = c_{p_k} T$. The subscript k in these equations represents chemical species k. Soret and Dufour effects as well as radiative heat transfer effects are not included in this model.

In this paper the pressure is related to the internal energy and species densities through the ideal gas equation of state

$$p = (\gamma - 1)\rho I \tag{7}$$

and the caloric equation of state

$$I = c_v T \ . \tag{8}$$

γ is the ratio of mixture specific heats, c_p/c_v, where

$$c_p = \rho^{-1} \sum_k \rho_k c_{p_k} \ ,$$

$$c_v = \rho^{-1} \sum_k \rho_k c_{v_k} \ , \quad \text{and} \quad c_{p_k} = c_{v_k} + R_o/w_k \ .$$

c_{p_k} and c_{v_k} are assumed constant in the calculations. Equations (7) and (8) differ from the forms used by some authors (see Ref. 8) since I is not the total specific internal energy I^*, but $I = I^* - \sum_k \left[h_{k_o} - c_{p_k} T_o\right] \left(\frac{\rho_k}{\rho}\right)$, where h_{k_o} is the standard heat of formation of species k at reference temperature T_o. Thus I is the specific internal energy less the energy of chemical bonding.

B. The Species Transport Equations.

The dynamics of the individual species are determined through the species transport equations:

$$\frac{\partial \rho_k}{\partial t} + \frac{1}{r}\frac{\partial \rho_k vr}{\partial r} + \frac{\partial \rho_k u}{\partial z} = \frac{1}{r}\frac{\partial}{\partial r}\left[\rho D_k r \frac{\partial}{\partial r}(\rho_k/\rho)\right] + \frac{\partial}{\partial z}\left[\rho D_k \frac{\partial}{\partial z}(\rho_k/\rho)\right] + (\dot{\rho}_k)_c$$

$$+ \frac{1}{r}\frac{\partial}{\partial r}\left(r\beta \frac{\partial \rho_k}{\partial r}\right) + \frac{\partial}{\partial z}\left(\beta \frac{\partial \rho_k}{\partial z}\right) \qquad (9)$$

Here $(\dot{\rho}_k)_c$ is the rate of change of species k density from chemical reactions given by

$$(\dot{\rho}_k)_c = w_k \sum_\ell R_\ell \left(B_k^\ell - A_k^\ell\right) \qquad (10)$$

in which R_ℓ is the rate of reaction ℓ. For the example calculations reported here, R_ℓ has the form:

$$R_\ell = C_\ell T^{n_\ell} e^{-E_\ell/R_o T} \prod_k \left(\frac{\rho_k}{w_k}\right)^{A_k^\ell} . \qquad (11)$$

The rate of heat release $\dot{q}_c$ in Eq. (4) is thus given by

$$\dot{q}_c = \sum_\ell R_\ell Q_\ell$$

where Q_ℓ, the heat release by reaction ℓ, is given by

$$Q_\ell = \sum_k w_k \left(A_k^\ell - B_k^\ell\right)\left(h_{k_o} - c_{p_k} T_o\right) . \qquad (12)$$

The molecular diffusion in Eq. (9) is modeled using Fick's Law. If we sum Eq. (9) over all species k and subtract Eq. (1), we obtain

$$\sum_k \left\{ \frac{1}{r} \frac{\partial}{\partial r} \left[\rho D_k r \frac{\partial}{\partial r} (\rho_k/\rho) \right] + \frac{\partial}{\partial z} \left[\rho D_k \frac{\partial}{\partial z} (\rho_k/\rho) \right] \right\} = 0 \qquad (13)$$

since mass is conserved by chemical reactions. Equation (13) is viewed as a constraint on the molecular diffusion coefficients D_k by the solution procedure.

TABLE I

DEFINITION OF SYMBOLS

Symbol	Definition
A_k^{ℓ}	Stoichiometric coefficient for species k as reactant in reaction ℓ*
B_k^{ℓ}	Stoichiometric coefficient for species k as product in reaction ℓ*
C_{ℓ}	Constant coefficient for reaction rate ℓ*
c_p	Mixture specific heat at constant pressure†
c_{p_k}	Specific heat of species k at constant pressure†
c_v	Mixture specific heat at constant volume†
c_{v_k}	Specific heat of species k at constant volume*
D_k	Mass diffusion coefficient for species k relative to mixture*
E_{ℓ}	Activation energy of reaction ℓ*
h_k	Specific enthalpy per unit mass of species k†
h_{k_o}	Heat of formation per unit mass of species k at temperature T_o*
I	Specific internal energy of mixture†
n_{ℓ}	Temperature exponent in reaction rate ℓ*
p	Equation of state pressure†
$\dot{q}_c$	Total rate of heat release per unit volume from chemical reactions†
Q_{ℓ}	Heat release of reaction ℓ†

TABLE I (Continued)

Symbol	Definition
q_r	Component of heat flux vector in radial direction†
q_z	Component of heat flux vector in axial direction†
r	Radial distance from symmetry axis†
R_ℓ	Reaction rate of reaction ℓ†
R_o	Universal gas constant*
T	Mixture temperature†
T_o	Fixed reference temperature*
u	Component of mixture velocity in axial direction†
v	Component of mixture velocity in radial direction†
w_k	Molecular weight of species k*
β	Turbulent eddy diffusivity*
γ	Mixture ratio of specific heats†
K	Thermal conductivity*
λ	Second coefficient of viscosity*
μ	First coefficient of viscosity*
ρ	Mixture density†
ρ_k	Density of species k†
σ_{rr}, σ_{rz} σ_{zz}, $\sigma_{\phi\phi}$	Components of viscous stress tensor†

*Quantities input to RICE.
†Quantities computed by RICE.

III. THE RICE SOLUTION PROCEDURE

In this section, we describe briefly the RICE computational mesh and the solution procedure through one time step; complete details are found in Ref. 4. The central feature of the RICE solution procedure is the use of the ICE[5] method. By eliminating the Courant sound speed restriction on the magnitude of the calculational time step, the method increases computational efficiency and automatically permits the solution of flows with materials speeds that range from far subsonic to supersonic.

The computing mesh is made up of a number of zones of rectangular cross section called cells. In each cell, of uniform dimensions δr and δz, are stored the computed variables describing the local fluid conditions. Figure 1 indicates the spatial locations of these variables within a cell indexed (i,j). The velocities and momentum densities are defined at cell edges; other quantities (denoted by $\psi_{i,j}$) are cell centered.

A simplified flow diagram for RICE appears in Fig. 2. To start the calculation, the input variables denoted in Table I are specified together with the initial values of the species densities, velocity components, and specific internal energy for each cell. Appropriate boundary conditions[9] are also specified.

First, the cell pressures and square of the adiabatic sound speed are computed using the polytropic gas equation of state:

$$p_{i,j} = (\gamma-1)\,\rho_{i,j}\,I_{i,j}$$

$$(c^2)_{i,j} = \gamma(\gamma-1)\,I_{i,j}$$

in which γ is defined as the ratio of the mass weighted specific heats of the mixture in the cell.

The coupled mass and momentum equations are next solved in the two-step ICE procedure. First, intermediate or tilde values of the mixture density and momentum densities are computed explicitly. Then an iterative scheme is used to solve for the advanced time density and velocities.

The tilde values of the mixture density are computed according to

$$\begin{aligned}\tilde{\rho}_{i,j} = \rho^n_{i,j} + \delta t \Bigg[(1-\theta)\Bigg\{&\frac{1}{r_j \delta r}\left[(\rho v)^n_{i,j-\frac{1}{2}}\, r_{j-\frac{1}{2}} - (\rho v)^n_{i,j+\frac{1}{2}}\, r_{j+\frac{1}{2}}\right] \\ &+ \frac{1}{\delta z}\left[(\rho u)^n_{i-\frac{1}{2},j} - (\rho u)^n_{i+\frac{1}{2},j}\right]\Bigg\} \\ &+ \frac{1}{r_j(\delta r)^2}\left[r_{j+\frac{1}{2}}\,\beta_{i,j+\frac{1}{2}}\left(\rho^n_{i,j+1} - \rho^n_{i,j}\right) - r_{j-\frac{1}{2}}\,\beta_{i,j-\frac{1}{2}}\left(\rho^n_{i,j} - \rho^n_{i,j-1}\right)\right] \\ &+ \frac{1}{(\delta z)^2}\left[\beta_{i+\frac{1}{2},j}\left(\rho^n_{i+1,j} - \rho^n_{i,j}\right) - \beta_{i-\frac{1}{2},j}\left(\rho^n_{i,j} - \rho^n_{i-1,j}\right)\right] \\ &+ \frac{1}{r_j(\delta r)^2}\left[r_{j+\frac{1}{2}}\,\tau_{i,j+\frac{1}{2}}\left(\rho^n_{i,j+1} - \rho^n_{i,j}\right) - r_{j-\frac{1}{2}}\,\tau_{i,j-\frac{1}{2}}\left(\rho^n_{i,j} - \rho^n_{i,j-1}\right)\right] \\ &+ \frac{1}{(\delta z)^2}\left[\tau_{i+\frac{1}{2},j}\left(\rho^n_{i+1,j} - \rho^n_{i,j}\right) - \tau_{i-\frac{1}{2},j}\left(\rho^n_{i,j} - \rho^n_{i-1,j}\right)\right]\Bigg] . \qquad (14)\end{aligned}$$

The superscript n is used to denote the value of the quantity at the time $t = n\delta t$. θ is a parameter used to vary the relative time centering of the convection terms. It ranges in value from zero for a purely explicit calculation to 1.0 for a completely time-advanced treatment of the convec-

tion terms. A value $\theta = 0.5$ is usually chosen for most compressible flow calculations because this value time centers the terms and eliminates the first order time errors that arise in the difference procedure.

The additional diffusion terms involving τ are added to cancel low order diffusional truncation errors. These errors may either lead to numerical instability or, alternatively, may lead to excessive diffusion in the calculated solution. The τ terms are calculated from the values of τ' given by

$$(\tau')_{i,j+\frac{1}{2}} = -(2\theta-1)\,\frac{\delta t}{2}\left\{\left(v^n_{i,j+\frac{1}{2}}\right)^2 + \frac{1}{2}\left[(c^2)^n_{i,j} + (c^2)^n_{i,j+1}\right]\right\}$$

$$+ \frac{\delta r}{\delta r_{j+\frac{1}{2}}}\left(r_{j+3/2}\, v^n_{i,j+3/2} - r_{j-\frac{1}{2}}\, v^n_{i,j-\frac{1}{2}}\right),$$

$$(\tau')_{i+\frac{1}{2},j} = -(2\theta-1)\,\frac{\delta t}{2}\left\{\left(u^n_{i+\frac{1}{2},j}\right)^2 + \frac{1}{2}\left[(c^2)^n_{i,j} + (c^2)^n_{i+1,j}\right]\right\}$$

$$+ \frac{\delta z}{\delta}\left(u^n_{i+3/2,j} - u^n_{i-\frac{1}{2},j}\right) . \qquad (15)$$

The value of τ is determined from the algebraic sign of τ',

$$\tau^n_{i,j+\frac{1}{2}} \begin{cases} (1+\xi)\,(\tau')_{i,j+\frac{1}{2}} & \text{if } (\tau')_{i,j+\frac{1}{2}} \geq 0 \\ (1-\xi)\,(\tau')_{i,j+\frac{1}{2}} & \text{if } (\tau')_{i,j+\frac{1}{2}} < 0 , \end{cases} \qquad (16)$$

where ξ is a constant ranging between zero and unity. The other values of τ' and τ are found similarly.

By controlling the magnitude of the low order diffusional truncation errors, this truncation error cancellation procedure[6,7] improves the accuracy and stability of the calculations. Controlling these errors is particularly advantageous for combusting flows because excessive numerical diffusion can be larger than the physical diffusivities, leading to inaccurate flame propagation speeds. A similar treatment to that given in Eqs. (14)-(16) is used for each of the RICE transport equations. For simplicity, we include them in this discussion only for the mixture continuity equation, to indicate the form and the manner in which the terms are included in the finite difference equations. A complete derivation is given in Ref. 7.

Omitting the truncation error terms, the radial momentum density is given by

$$
\begin{aligned}
(\widetilde{\rho v})_{i,j+\frac{1}{2}} = (\rho v)^n_{i,j+\frac{1}{2}} + \delta t \Bigg[& \frac{1}{r_{j+\frac{1}{2}}\delta r} \Big\{ r_j \left[(\rho v^2)_{i,j} - (\sigma_{rr})_{i,j} \right] \\
& - r_{j+1} \left[(\rho v^2)_{i,j+1} - (\sigma_{rr})_{i,j+1} \right] \Big\} \\
& + \frac{1}{\delta z} \left[(\rho uv)_{i-\frac{1}{2},j+\frac{1}{2}} - (\sigma_{rz})_{i-\frac{1}{2},j+\frac{1}{2}} - (\rho uv)_{i+\frac{1}{2},j+\frac{1}{2}} + (\sigma_{rz})_{i+\frac{1}{2},j+\frac{1}{2}} \right] \\
& + \frac{1}{\delta r} \left(p^n_{i,j} - p^n_{i,j+1} \right) \\
& - \frac{1}{r_{j+\frac{1}{2}}} (\sigma_{\phi\phi})_{i,j+\frac{1}{2}} + v^n_{i,j+\frac{1}{2}} \Bigg\{ \frac{1}{2r_{j+\frac{1}{2}}(\delta r)^2} \left[r_{j+1} \beta_{i,j+1} \left(\rho^n_{i,j+2} - \rho^n_{i,j} \right) \right. \\
& \left. - r_j \beta_{i,j} \left(\rho^n_{i,j+1} - \rho^n_{i,j-1} \right) \right]
\end{aligned}
$$

$$+\frac{1}{(\delta z)^2}\left[\beta_{i+\frac{1}{2},j+\frac{1}{2}}\left(\rho_{i+1,j+\frac{1}{2}}-\rho_{i,j+\frac{1}{2}}\right)-\beta_{i-\frac{1}{2},j+\frac{1}{2}}\left(\rho_{i,j+\frac{1}{2}}-\rho_{i-1,j+\frac{1}{2}}\right)\right]\Bigg\}$$

$$+\frac{1}{2}\left(\rho^n_{i,j}+\rho^n_{i,j+1}\right)\beta_{i,j+\frac{1}{2}}\left\{\frac{1}{(\delta r)^2}\left(v^n_{i,j+3/2}-2v^n_{i,j+\frac{1}{2}}+v^n_{i,j-\frac{1}{2}}\right)\right.$$

$$\left.+\frac{1}{(\delta z)^2}\left(v^n_{i+1,j+\frac{1}{2}}-2v^n_{i,j+\frac{1}{2}}+v^n_{i-1,j+\frac{1}{2}}\right)\right\}\Bigg] \qquad (17)$$

Here, straightforward centered differences and averages at time level n are used for the various terms indicated. A similar equation is solved for $(\tilde{\rho u})_{i+\frac{1}{2},j}$.

With $\tilde{\rho}$, $\tilde{\rho v}$, and $\tilde{\rho u}$ computed, the finite difference approximations for the time advanced density and momenta become:

$$\rho^{n+1}_{i,j}=\tilde{\rho}_{i,j}+\theta\delta t\left\{\frac{1}{r_j\delta r}\left[(\rho v)^{n+1}_{i,j-\frac{1}{2}}\,r_{j-\frac{1}{2}}-(\rho v)^{n+1}_{i,j+\frac{1}{2}}\,r_{j+\frac{1}{2}}\right]\right.$$

$$\left.+\frac{1}{\delta x}\left[(\rho u)^{n+1}_{i-\frac{1}{2},j}-(\rho u)^{n+1}_{i+\frac{1}{2},j}\right]\right\}, \qquad (18)$$

$$(\rho v)^{n+1}_{i,j+\frac{1}{2}}=(\tilde{\rho v})_{i,j+\frac{1}{2}}+\frac{\phi\delta t}{\delta r}\left(\delta\bar{p}_{i,j}-\delta\bar{p}_{i,j+1}\right) \qquad (19)$$

and

$$(\rho u)^{n+1}_{i+\frac{1}{2},j}=(\tilde{\rho u})_{i+\frac{1}{2},j}+\frac{\phi\delta t}{\delta x}\left(\delta\bar{p}_{i,j}-\delta\bar{p}_{i+1,j}\right). \qquad (20)$$

The $\delta\bar{p}$'s are advanced time pressure increments that reflect pressure changes resulting from adiabatic compressions. The role of ϕ is similar to that of θ in Eq. (14).

The solution of Eqs. (18)-(20) is accomplished by iterating on the pressure $\bar{p}_{i,j}=p^n_{i,j}+\delta\bar{p}_{i,j}$. The criterion for convergence of the

iteration procedure is that the mixture continuity equation, Eq. (18), is satisfied to within a specified small amount ε; that is, Eq. (18) is written as

$$D_{i,j} = \rho^{n+1}_{i,j} - \tilde{\rho}_{i,j} - \theta\delta t \left\{ \frac{1}{r_j \delta r}\left[r_{j-\frac{1}{2}} (\rho v)^{n+1}_{i,j-\frac{1}{2}} - r_{j+\frac{1}{2}} (\rho v)^{n+1}_{i,j+\frac{1}{2}}\right] + \frac{1}{\delta z}\left[(\rho u)^{n+1}_{i-\frac{1}{2},j} - (\rho u)^{n+1}_{i+\frac{1}{2},j}\right]\right\} \tag{21}$$

and the convergence requirement is $|D_{i,j}| < \varepsilon$ for all cells (i,j). The iteration is started using densities and pressures at time level n and tilde values of the momentum densities.

If the convergence criterion for cell (i,j) is satisfied, the pressure, density, and momenta of cell (i,j) are not changed. If, however, the criterion is not met, the pressure is changed by an amount

$$\delta\bar{p}_{i,j} = -\frac{\Omega D_{i,j}}{\left(\frac{\partial D}{\partial \bar{p}}\right)_{i,j}}$$

where

$$\left(\frac{\partial D}{\partial \bar{p}}\right)_{i,j} = \frac{1}{(c^2)_{i,j}} + 2\theta\phi\, \delta t^2 \left(\frac{1}{\delta r^2} + \frac{1}{\delta z^2}\right)$$

and Ω is a constant over-relaxation factor usually chosen in the range $1.0 \leq \Omega < 2.0$. The values of the cell quantities are then changed as follows:

$$\overline{p}^{n+1}_{i,j} \leftarrow \overline{p}^{n+1}_{i,j} + \delta\overline{p}_{i,j}$$

$$\rho^{n+1}_{i,j} \leftarrow \rho^{n+1}_{i,j} + \delta\overline{p}_{i,j}/(c^2)_{i,j}$$

$$(\rho u)^{n+1}_{i+\frac{1}{2},j} \leftarrow (\rho u)^{n+1}_{i+\frac{1}{2},j} + \frac{\phi\delta t}{\delta z}\,\delta\overline{p}_{i,j}$$

$$(\rho u)^{n+1}_{i+\frac{1}{2},j} \leftarrow (\rho u)^{n+1}_{i-\frac{1}{2},j} - \frac{\phi\delta t}{\delta z}\,\delta\overline{p}_{i,j}$$

$$(\rho v)^{n+1}_{i,j+\frac{1}{2}} \leftarrow (\rho v)^{n+1}_{i,j+\frac{1}{2}} + \frac{\phi\delta t}{\delta r}\,\delta\overline{p}_{i,j}$$

$$(\rho v)^{n+1}_{i,j-\frac{1}{2}} \leftarrow (\rho v)^{n+1}_{i,j-\frac{1}{2}} - \frac{\phi\delta t}{\delta r}\,\delta\overline{p}_{i,j}\ . \qquad (22)$$

After the criterion is met for each cell, the advanced time velocities are obtained by

$$u^{n+1}_{i+\frac{1}{2},j} = \frac{2\,(\rho u)^{n+1}_{i+\frac{1}{2},j}}{\rho^{n+1}_{i,j} + \rho^{n+1}_{i+1,j}}$$

$$v^{n+1}_{i,j+\frac{1}{2}} = \frac{2\,(\rho v)^{n+1}_{i,j+\frac{1}{2}}}{\rho^{n+1}_{i,j} + \rho^{n+1}_{i,j+1}}\ .$$

These velocities and pressures are then used in an explicit calculation of the internal energy, neglecting changes in internal energy due to chemical heat release and enthalpy diffusion:

$$(\overline{\rho I})_{i,j} = (\rho I)^n_{i,j} + \delta t \left\{ \frac{1}{r_j \delta r} \left[r_{j-\frac{1}{2}} (\rho I)_{i,j-\frac{1}{2}} v^{n+1}_{i,j-\frac{1}{2}} - r_{j+\frac{1}{2}} (\rho I)_{i,j+\frac{1}{2}} v^{n+1}_{i,j+\frac{1}{2}} \right] \right.$$

$$+ \frac{1}{\delta z} \left[(\rho I)_{i-\frac{1}{2},j} u^{n+1}_{i-\frac{1}{2},j} - (\rho I)_{i+\frac{1}{2},j} u^{n+1}_{i+\frac{1}{2},j} \right]$$

$$- \bar{p}_{i,j} \left[\frac{1}{r_j \delta r} \left(r_{j+\frac{1}{2}} v^{n+1}_{i,j+\frac{1}{2}} - r_{j-\frac{1}{2}} v^{n+1}_{i,j-\frac{1}{2}} \right) + \frac{1}{\delta z} \left(u^{n+1}_{i+\frac{1}{2},j} - u^{n+1}_{i-\frac{1}{2},j} \right) \right]$$

$$+ (\sigma_{rr})_{i,j} \frac{1}{\delta r} \left(v^{n+1}_{i,j+\frac{1}{2}} - v^{n+1}_{i,j-\frac{1}{2}} \right)$$

$$+ (\sigma_{rz})_{i,j} \left[\frac{1}{\delta r} \left(u_{i,j+\frac{1}{2}} - u_{i,j-\frac{1}{2}} \right) + \frac{1}{\delta z} \left(v_{i+\frac{1}{2},j} - v_{i-\frac{1}{2},j} \right) \right]$$

$$+ (\sigma_{zz})_{i,j} \frac{1}{\delta z} \left(u^{n+1}_{i+\frac{1}{2},j} - u^{n+1}_{i-\frac{1}{2},j} \right) + (\sigma_{\phi\phi})_{i,j} \frac{1}{r_j} v_{i,j}$$

$$+ \frac{1}{r_j (\delta r)^2} \left[r_{j+\frac{1}{2}} \kappa_{i,j+\frac{1}{2}} \left(T^n_{i,j+1} - T^n_{i,j} \right) - r_{j-\frac{1}{2}} \kappa_{i,j-\frac{1}{2}} \left(T^n_{i,j} - T^n_{i,j-1} \right) \right]$$

$$+ \frac{1}{(\delta z)^2} \left[\kappa_{i+\frac{1}{2},j} \left(T^n_{i+1,j} - T^n_{i,j} \right) - \kappa_{i-\frac{1}{2},j} \left(T^n_{i,j} - T^n_{i-1,j} \right) \right]$$

$$+ I^n_{i,j} \left[\frac{1}{r_j (\delta r)^2} \left[r_{j+\frac{1}{2}} \beta_{i,j+\frac{1}{2}} \left(\rho^{n+1}_{i,j+1} - \rho^{n+1}_{i,j} \right) - r_{j-\frac{1}{2}} \beta_{i,j-\frac{1}{2}} \left(\rho^{n+1}_{i,j} - \rho^{n+1}_{i,j-1} \right) \right] \right.$$

$$\left. + \frac{1}{(\delta z)^2} \left[\beta_{i+\frac{1}{2},j} \left(\rho^{n+1}_{i+1,j} - \rho^{n+1}_{i,j} \right) - \beta_{i-\frac{1}{2},j} \left(\rho^{n+1}_{i,j} - \rho^{n+1}_{i-1,j} \right) \right] \right]$$

$$\left. + \rho^{n+1}_{i,j} \beta_{i,j} \left[\frac{1}{(\delta r)^2} \left(I^n_{i,j+1} - 2I^n_{i,j} + I^n_{i,j-1} \right) + \frac{1}{(\delta z)^2} \left(I^n_{i+1,j} - 2I^n_{i,j} + I^n_{i-1,j} \right) \right] \right\} \tag{23}$$

in which

$$I^n_{i,j} = \frac{(\rho I)^n_{i,j}}{\rho^n_{i,j}}$$

and from Eq. (8)

$$T^n_{i,j} = \frac{(\rho I)^n_{i,j}}{\sum_k (\rho_k)_{i,j} (c_v)_k} \quad .$$

Next, the changes in species densities for the time step are obtained. The finite difference approximation to the species transport equation, Eq. (9), is accomplished by calculating incremental changes in ρ_k first for the convective process, next for the laminar and/or turbulent diffusion, and finally for the chemical rates. The order in which these increments are computed is arbitrary. We have switched the order and found no significant changes in the calculated results for the problems that have been computed thus far.

The species convection portion is given by

$$(\bar{\rho}_k)_{i,j} = (\rho_k)^n_{i,j} + \delta t \left\{ \frac{1}{r_j \delta r} \left[r_{j-\frac{1}{2}} (\rho_k v)_{i,j-\frac{1}{2}} - r_{j+\frac{1}{2}} (\rho_k v)_{i,j+\frac{1}{2}} \right] \right.$$

$$\left. + \frac{1}{\delta z} \left[(\rho_k u)_{i-\frac{1}{2},j} - (\rho_k u)_{i+\frac{1}{2},j} \right] \right\} , \qquad (24)$$

where, for example,

$$(\rho_k v)_{i,j+\frac{1}{2}} = \frac{1}{2} \left\{ (\rho_k)^n_{i,j} + (\rho_k)^n_{i,j+1} - \frac{\delta t}{\delta r} \left[(\rho_k)^n_{i,j+1} - (\rho_k)^n_{i,j} \right] v^{n+1}_{i,j+\frac{1}{2}} \right\} v^{n+1}_{i,j+\frac{1}{2}} .$$

Straightforward centered differences are used in the finite difference approximation to Eq. (13) for the laminar mixing portion. Turbulent diffusion of the species is treated in an analogous way to that in Eq. (14) with ρ_k substituted for ρ in the appropriate terms. Chemical reactions are computed for each cell as detailed in Eqs. (10)-(11) using an implicit approach to prevent the reactant species from becoming negative in value during the time step. For reaction times that are short compared to the characteristic times for hydrodynamic motion, a submultiple of the fluid dynamic time step is used for the chemistry portion to more accurately represent the kinetics. Finally, the mixture internal energy equation is updated for the time step to reflect the net heat release given by Eq. (12) and for enthalpy diffusion.

IV. ARTIFICIAL THICKENING OF DEFLAGRATION WAVES

In this section we introduce a technique for artificially thickening deflagration waves to dimensions resolvable by typical cell sizes used in two dimensional calculations. A difficulty with numerical solutions involving deflagrations is that the physical thickness of a laminar flame front is very small compared to the computational cell sizes it is practical to use in two dimensional calculations. One solution to this problem is to treat the deflagration wave as a discontinuity. This procedure can become computationally time consuming, especially when the burn front curls over on itself or breaks apart due to the presence of obstacles in the flow field. (See the second example calculation presented in this paper.) The artificial thickening technique takes little computer time, and no additional logic is required to model difficult interface geometries. Its disadvantage is that it may suppress or alter the growth rate of fluid dynamic instabilities with wavelengths comparable to the deflagration wave thickness.

The mathematical justification for the artificial thickening procedure follows from a simple coordinate transformation argument. We consider a steady-state, one dimensional, laminar flame front whose density profile is shown schematically in the top portion of Fig. 3, and another solution, shown in the bottom part, which is obtained by expanding the coordinates in the vicinity of the flame front through an appropriate mapping function $\chi(x)$. It may be rigorously verified that the expanded solution satisfies the equations of motion in the new coordinate system if all diffusivities are multiplied by χ' and all reaction rates are divided by χ', where χ' is the derivative of χ with respect to x.

Hence, by increasing diffusivities by the factor χ' and decreasing reaction rates by the factor of $1/\chi'$, the rate of propagation of the deflagration wave remains the same while its thickness is increased by a factor of χ'. χ' can vary spatially so that by making χ' large only in the vicinity of the flame front, its effects are localized in a manner similar to the effect of artificial dissipation terms in the numerical treatment of shock waves.

An example of the use of this procedure is presented in the next section.

V. NUMERICAL EXAMPLES

One Dimensional Steady-State Deflagration

To illustrate the effectiveness of the artificial thickening technique described in Sec. IV, we applied RICE to the one-dimensional, laminar, steady combustion of gaseous species A to form species B. The calculated solution achieves steady state through transient processes.

In the calculations, A enters the computing region from the left at atmospheric pressure and temperature with velocity 370 cm/s and density 1.0×10^{-3} g/cm^3. It reacts to form B according to the simple reaction

$$2A \rightarrow B$$

with a heat release $Q_\ell = 580$ cal/g and at the rate defined in Eq. (11) in which

$$C_\ell = 4.9 \times 10^{12} \frac{cm^3}{g\text{-}s}$$

$$n_\ell = 0.0$$

and $E_\ell = 1.0 \times 10^{12}$ ergs/mole.

The right boundary of the mesh is an outflow boundary in which species B exits the mesh with density $\rho_\infty = 1.2 \times 10^{-4}$ g/cm^3 and velocity 3.0×10^5 cm/s.

The diffusivities for the species are given by

$$\mu = 1.1 \times 10^{-5} \sqrt{T} \frac{g}{cm\text{-}s}$$

$$D_A = D_B = 2.9 \times 10^{-5} \sqrt{T} / (2\rho_A + \rho_B) \frac{cm^2}{s}$$

and $\kappa/c_{v_A} = 1.5 \times 10^{-5} \sqrt{T} \ \frac{g}{cm\text{-}s}$

Typical thicknesses for laminar diffusion flames are approximately 1×10^{-2} cm, negliglible compared to the calculational cell size $\delta z = 1$ cm.

Shown in Fig. 4 are plots of the fluid density versus distance at steady state for two different values of χ'. The dashed line is the theoretical profile. The value of $\chi' = 1.0 \times 10^{3}$ smears the flame over approximately 5 computational zones, while $\chi' = 4.0 \times 10^{5}$ thickens the flame to approximately 20 computational zones. In both cases, the calculations retain the correct flame speed and the correct jump conditions across the flame front.

We note that the time step for the $\chi' = 1.0 \times 10^{3}$ case is $\delta t = 1.5 \times 10^{-4}$ sec which results in a Courant number based on sound speed of 16. This illustrates the advantage of the implicit ICE technique in permitting the use of larger time steps than are attainable by explicit methods.

Turbulent Combustion in Connected Closed Chambers.

As an example of two-dimensional, unsteady combustion, we applied RICE to the turbulent combustion inside two connected closed chambers. For this calculation, gaseous species A reacted to form B as in the previous example with

$$C_\ell = 2.0 \times 10^{12} \ \frac{cm^3}{g\text{-}s}$$

$$n_\ell = 0.0$$

$$E_\ell = 1.25 \times 10^{12} \ \frac{ergs}{mole}$$

and $Q_\ell = 5.0 \times 10^2 \frac{cal}{g}$.

The axisymmetric configuration (see Fig. 5) is that of a small chamber of inside radius 0.7 cm and 1.4 cm axial length connected through an inlet 0.3 cm in radius and 1.0 cm in length to the main chamber 3.0 cm in radius and 1.8 cm in length. The computational cells are of uniform size with $\delta r = 0.1$ cm and $\delta z = 0.2$ cm. The chamber boundaries are represented as rigid, free-slip, adiabatic walls. For this problem, the turbulent diffusivity is constant, $\beta = 1.0 \times 10^2$ cm^2/s, and the laminar diffusivities are zero.

Initially both chambers and the inlet were uniformly filled with species A at density $\rho = 1.0 \times 10^{-3}$ g/cm^3, T = 300°K, and $p = 1.0 \times 10^6 \frac{dynes}{cm^2}$. Initiation of combustion was accomplished by the deposition of $1.8 \times 10^{12} \frac{ergs}{cm^3 . s}$ in four calculational cells adjacent to the symmetry axis at the left hand side of the small chamber until $t = 1.0 \times 10^{-5}$ s.

Figure 5 summarizes the results of the calculation by showing side-by-side the cross-sections of the velocity vectors and contour plots of species density at four different times: t = 1,2,4, and 5×10^{-4} s, chronologically, from top to bottom. The bottom boundary in each of these plots is the symmetry axis. The flame front is deduced from the density contour plots as the region of steep gradients.

At $t = 1.0 \times 10^{-4}$ s, the flame front is in the small chamber but a compression wave ahead of the flame has proceeded into the main chamber. At $t = 2.0 \times 10^{-4}$ s, the front has advanced rapidly in the axial direction due to the large convective velocities of the inlet jet. The velocity

vectors show the presence of a large vortex formed as the jet collides with the right hand wall. Some burning is still occuring in the small chamber. The gases in the small chamber overexpand, and the frames for $t = 4.0 \times 10^{-4}$ s show the fluid velocities in the inlet have reversed direction and some reaction is taking place in the inlet. The flame front advances from right to left in the large chamber until the last time in which there is only a small parcel of species A remaining along the left wall of this chamber. Diagnostics at $t = 6 \times 10^{-4}$ s, the end of this calculation, show the reaction along the left wall almost complete. Total calculation time on a CDC 7600 computer was nine minutes.

REFERENCES

1. W. C. Rivard, T. D. Butler, and O. A. Farmer, "The Transient Dynamics of Chemically Reactive Gaseous Mixtures with Turbulence," Lecture Notes in Physics 35, Springer-Verlag, New York (1975) pp. 334-340.

2. T. D. Butler and P. J. O'Rourke, "Numerical Studies of the Interior Ballistics of Liquid Monopropellant Guns," Los Alamos Scientific Laboratory report (to be published).

3. F. V. Bracco, et.al., "Two-Phase, Two-Dimensional, Unsteady Combustion in Internal Combustion Engines; Preliminary Theoretical-Experimental Results," Society of Automotive Engineers Publication no. 760114 (February, 1976).

4. W. C. Rivard, O. A. Farmer, And T. D. Butler, "RICE: A Computer Program for Multicomponent Chemically Reactive Flows at All Speeds," Los Alamos Scientific Laboratory report LA-5812 (1975).

5. F. H. Harlow and A. A. Amsden, "A Numerical Fluid Dynamics Calculation Method for All Flow Speeds," J. Comp. Phys. 8, 197-213 (1971).

6. C. W. Hirt, "Heuristic Stability Theory for Finite Difference Equations," J. Comp. Phys. 2, 339-354 (1968).

7. W. C. Rivard, T. D. Butler, O. A. Farmer, and P. J. O'Rourke, "A Method for Increased Accuracy in Eulerian Fluid Dynamics Calculations," Los Alamos Scientific Laboratory report LA-5426-MS (1973).

8. F. A. Williams, Combustion Theory, Addison-Wesley Publishing Company, Inc., pp. 2-4 (1965).

9. T. D. Butler, "Recent Advances in Computational Fluid Dynamics," Computing Methods in Applied Sciences and Engineering, Part 2, Lecture Notes in Computer Science No. 11 (1974).

FIGURE CAPTIONS

Fig. 1. Schematic diagram of a RICE computational cell showing the locations where flow quantities are defined.

Fig. 2. Abbreviated flow chart for the RICE code.

Fig. 3. Representation of steady state deflagration wave solution ρ and its transformed solution.

Fig. 4. Steady state density versus distance profiles obtained by RICE for one-dimensional deflagration calculations.

Fig. 5. Velocity vector and reactant density contour plots at times t = 1.0, 2.0, 4.0, and 5.0 x 10^{-4} s, from top to bottom, for the calculation of unsteady combustion in two connected, closed chambers.

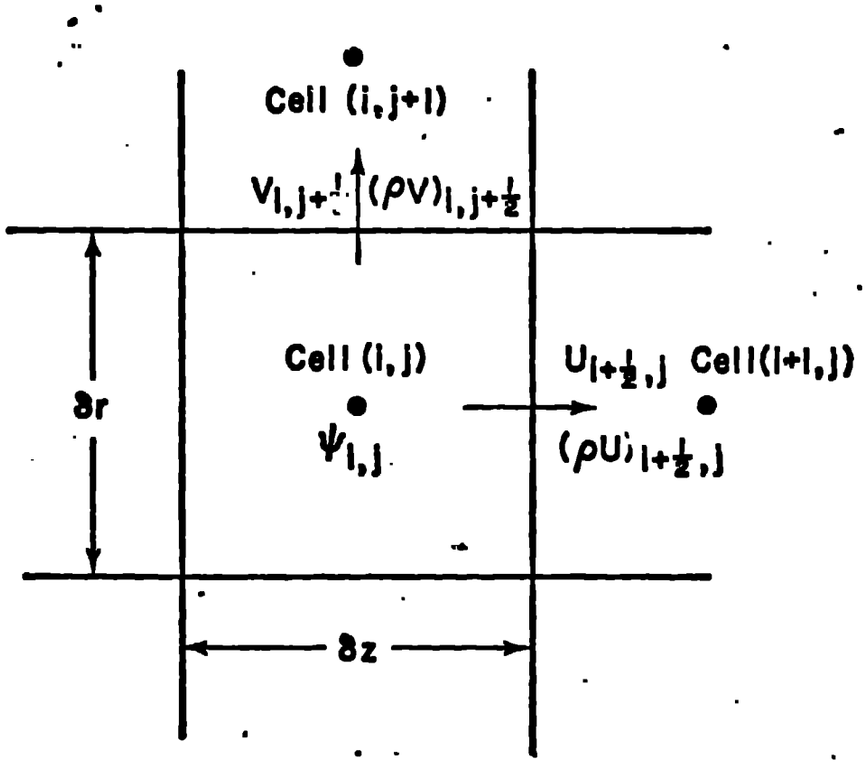
Cell (i,j+1)
$V_{I,j+\frac{1}{2}}$
$(\rho V)_{I,j+\frac{1}{2}}$
Cell (I,j)
$U_{I+\frac{1}{2},j}$
Cell(I+1,j)
δr
$\psi_{I,j}$
$(\rho U)_{I+\frac{1}{2},j}$
δz

Fig. 1

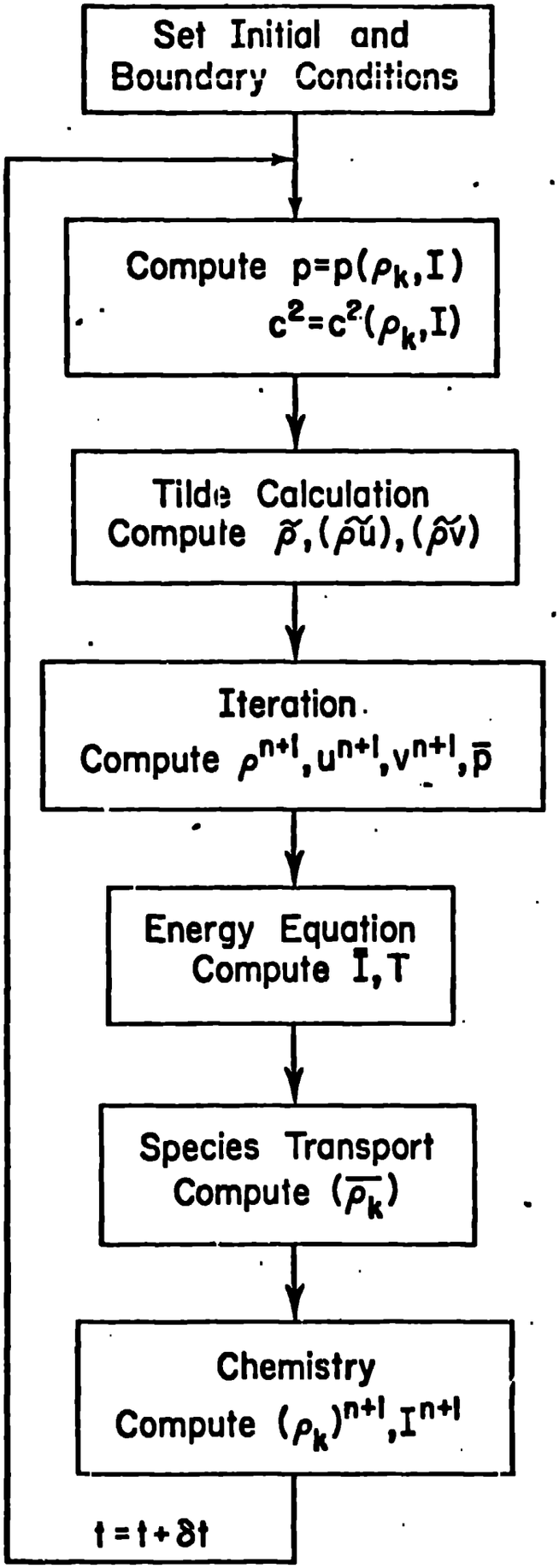
Set Initial and Boundary Conditions
Compute $p=p(\rho_k,I)$ $c^2=c^2(\rho_k,I)$
Tilde Calculation Compute $\tilde{\rho},(\widetilde{\rho u}),(\widetilde{\rho v})$
Iteration. Compute $\rho^{n+1},u^{n+1},v^{n+1},\bar{p}$
Energy Equation Compute $\bar{I},T$
Species Transport Compute $(\overline{\rho_k})$
Chemistry Compute $(\rho_k)^{n+1},I^{n+1}$
$t=t+\delta t$

Fig. 2

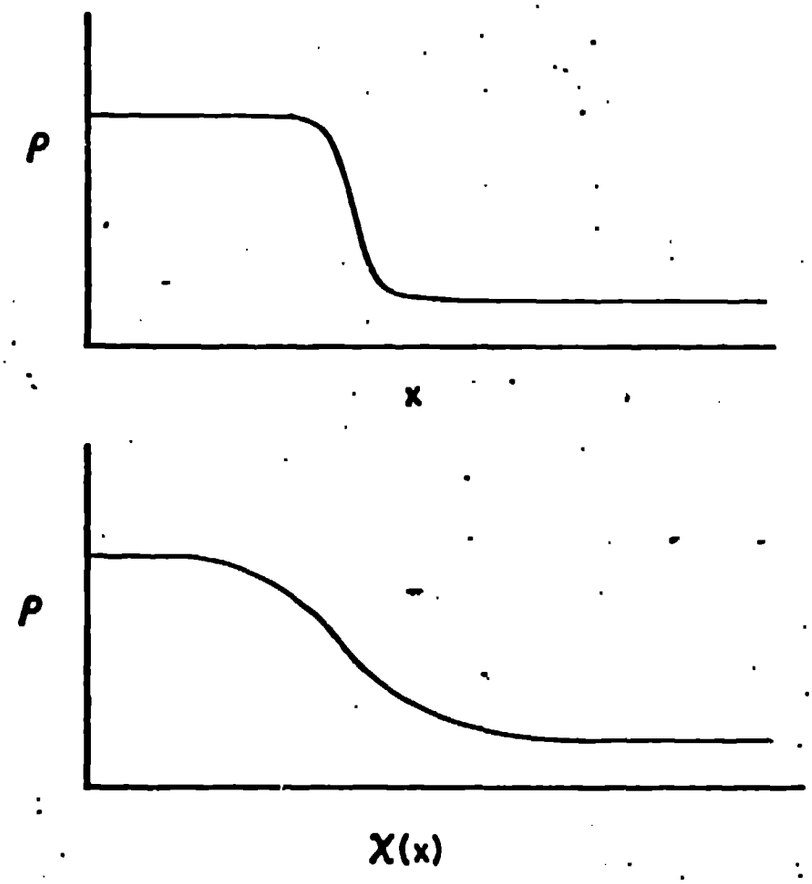

Fig. 3

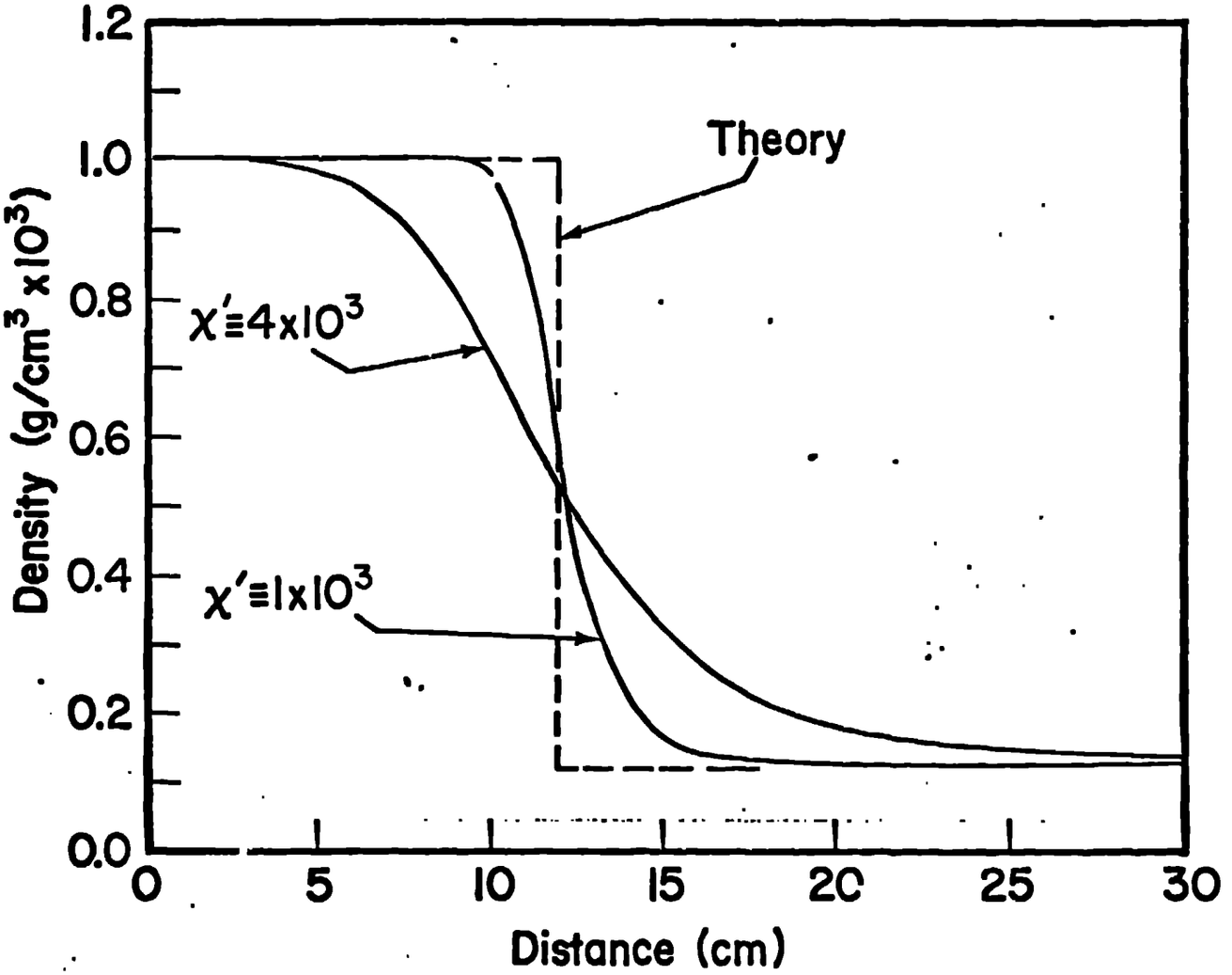

Fig. 4

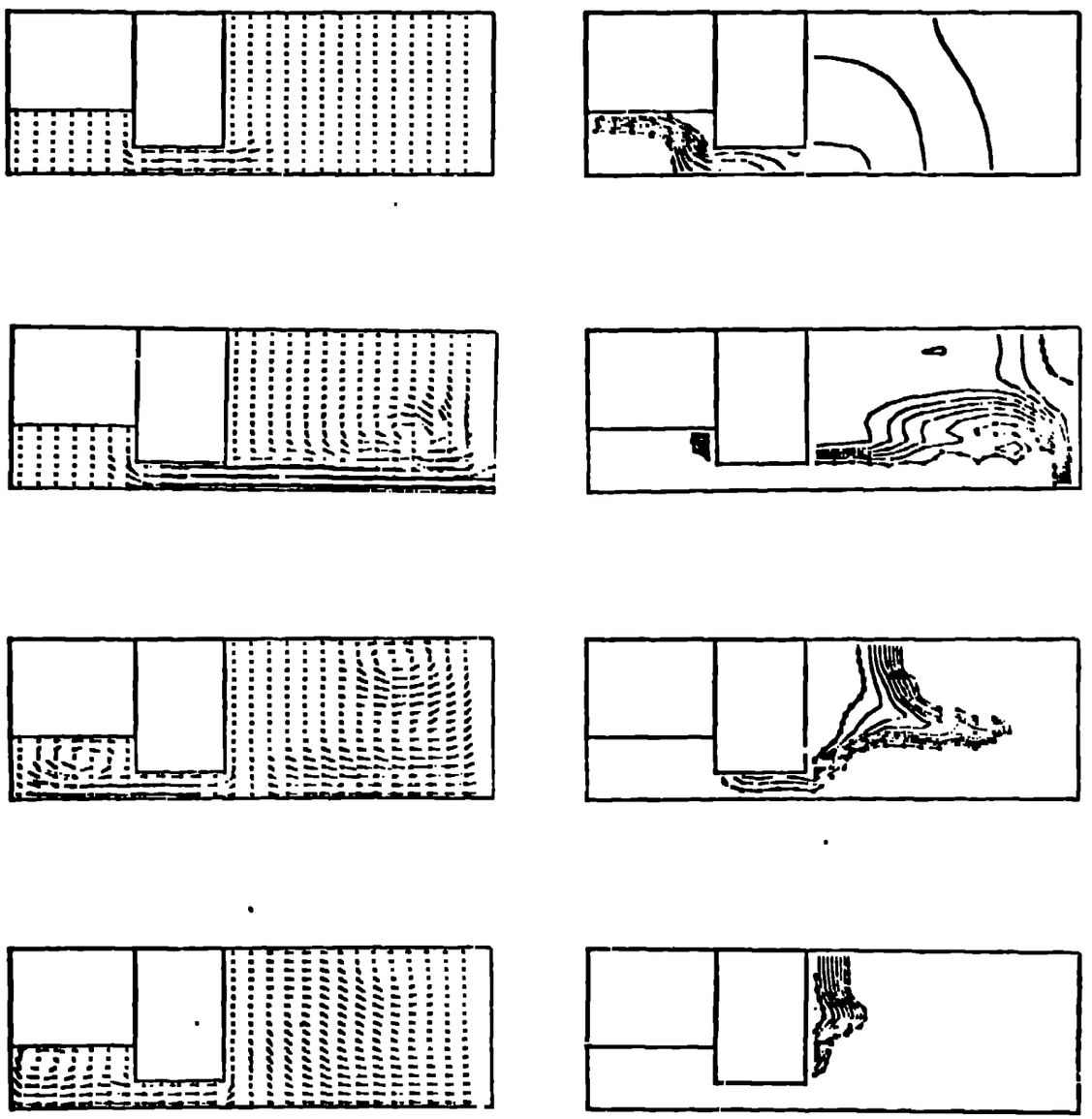

Fig. 5